

Percolation and Criticality in Hyperuniform Networks

Yongyi Wang,¹ Jaeuk Kim,² Yang Jiao,^{3,4} Izabella
Stuhl,⁵ Salvatore Torquato,^{6,2,7,8} and Reka Albert^{1,*}

¹*Department of Physics, Pennsylvania State University, University Park, PA 16802*

²*Department of Physics, Princeton University,
Princeton, New Jersey 08544, USA*

³*Materials Science and Engineering,
Arizona State University, Tempe, AZ 85287*

⁴*Department of Physics, Arizona State University, Tempe, AZ 85287*

⁵*Department of Mathematics, Pennsylvania State University, University Park, PA 16802*

⁶*Department of Chemistry, Princeton University,
Princeton, New Jersey 08544, USA*

⁷*Princeton Institute of Materials, Princeton University,
Princeton, New Jersey 08544, USA*

⁸*Program in Applied and Computational Mathematics,
Princeton University, Princeton, New Jersey 08544, USA*

(Dated: March 18, 2026)

Abstract

Hyperuniform many-particle systems, which encompass crystals, quasicrystals and certain exotic disordered systems, exhibit an anomalous suppression of density fluctuations on macroscopic length scales relative to those of conventional disordered systems. Here we investigate the percolation behaviors of disordered stealthy hyperuniform systems, a subclass of hyperuniform configurations for which the structure factor vanishes for a finite range of wavevectors near the origin, with the degree of stealthiness controlled via a parameter χ . We construct Delaunay triangulation networks derived from stealthy hyperuniform configurations with varying χ as well as Poisson (uncorrelated) point configurations for the purpose of comparison. We investigate a non-uniform bond percolation process on the triangulation networks, in which bond occupation probabilities decrease with the Euclidean distance between the connected vertices. In this setting, percolation (i.e., emergence of a globally connected path) is induced by varying a tuning parameter z . We estimate the percolation thresholds z_c and critical exponents of the Delaunay triangulation networks via finite-size scaling and the Newman–Ziff Monte Carlo algorithm. We find that stealthy hyperuniform networks exhibit lower percolation thresholds than Poisson networks. Notably, the percolation threshold of stealthy hyperuniform networks decreases with the stealthiness parameter χ , indicating that system-spanning connectivity emerges more readily as short-range order increases. Moreover, we show that stealthy hyperuniform networks with large χ belong to the same universality class as regular lattices, while Poisson and low- χ systems show deviations from this universality class. We relate the shift in critical exponents to the degree of suppression of density fluctuations in the point configurations. Our work extends previous studies on transport properties of stealthy hyperuniform systems from continuum two-phase media to networks. These results open new avenues for optimizing the resilience of statistically homogeneous disordered networks.

I. INTRODUCTION

A *hyperuniform* many-particle system, disordered or not, is one in which the number variance of particle centers within a spherical observation window of radius R grows slower

* correspondence sent to: rza1@psu.edu

than the observation window volume R^d in d -dimensional space for large R [1, 2], i.e.,

$$\lim_{R \rightarrow \infty} \sigma_N^2(R)/v_1(R) = 0 \quad (1)$$

where $\sigma_N^2(R) \equiv \langle N(R)^2 \rangle - \langle N(R) \rangle^2$ is the variance in the number of particle centers (brackets indicate the ensemble average) and $v_1(R) \sim R^d$ is the volume of a d -dimensional sphere of radius R . Equivalently, a system is hyperuniform if its structure factor $S(\mathbf{k})$ (defined in Sec. II) tends to zero as the wavenumber $k \equiv |\mathbf{k}|$ tends to zero, i.e.,

$$\lim_{|\mathbf{k}| \rightarrow 0} S(\mathbf{k}) = 0. \quad (2)$$

The small- $|\mathbf{k}|$ scaling behavior of $S(\mathbf{k}) \sim |\mathbf{k}|^\alpha$ determines the large- R asymptotic behavior of $\sigma_N^2(R)$, based on which all hyperuniform systems, disordered or not, can be categorized into three classes: $\sigma_N^2(R) \sim R^{d-1}$ for $\alpha > 1$ (class I); $\sigma_N^2(R) \sim R^{d-1} \ln(R)$ for $\alpha = 1$ (class II); and $\sigma_N^2(R) \sim R^{d-\alpha}$ for $0 < \alpha < 1$ (class III) [2]. Consequently, hyperuniform systems encompass all crystals and quasicrystals [1, 2]. Hyperuniformity has also been identified in a wide spectrum of physical [3–31], material [32–47] and biological [48–52] systems. The unique combination of local disorder and complete suppression of global density fluctuations endows these systems with unexpected physical properties, including novel wave propagation characteristics [53–63], thermal, electrical and diffusive transport properties [64–66], mechanical properties [67, 68] as well as optimal multifunctional characteristics [69–71].

Stealthy hyperuniform systems, the focus of this work, are a special subset of class-I hyperuniform systems, which possess a zero structure factor for a range of wavevectors around the origin, i.e., $S(\mathbf{k}) = 0$ for $\mathbf{k} \in \Omega$ (excluding the forward scattering). The degree of stealthiness and short-range order of such systems are controlled by a tuning parameter χ , which measures the relative fraction of independently constrained wavevectors within the exclusion region Ω (see Sec. II for detailed definitions). In this work, we focus on the disordered regime, i.e., $0 < \chi < 1/2$, in which the systems possess no long-range order. Stealthy hyperuniform systems completely suppress density fluctuations from intermediate to infinite wavelengths, which is in contrast to standard hyperuniform systems that suppress density fluctuations only at the infinite wavelength. This unique structural feature endows disor-

dered stealthy hyperuniform systems with highly efficient transport characteristics despite the absence of crystalline order [64, 65, 69]. In particular, a previous study of continuum percolation in two-phase media found that stealthy hyperuniform two-phase media exhibit a higher percolation volume fraction than Poisson (uncorrelated) systems, with the threshold depending systematically on the stealthiness parameter χ [64].

We are thus motivated to investigate whether networks derived from stealthy hyperuniform point configurations, which are discrete rather than continuous mathematical objects, also exhibit distinct percolation properties. For the purpose of comparison, the same analysis is carried out for Poisson point configurations. We generate Delaunay triangulation networks, whose parameterless and planar nature is particularly well suited for analyzing the underlying spatial structure of point configurations [72], and study their percolation behaviors.

Previous studies on percolation of stealthy hyperuniform systems focused on continuum percolation of two-phase media by increasing the radius of congruent spheres centered at the points [64]. Our work departs from this continuum perspective by studying the connectivity of networks generated directly from stealthy hyperuniform point configurations. This distinction is important because, unlike continuum percolation where connectivity is deterministic for a given disordered realization [73, 74], percolation on networks also involves stochastic connectivity arising from probabilistic bond occupation. Such stochastic bond percolation models have been widely used to model resilience and robustness in complex networks, including infrastructure and biological systems [75–78].

We examine a distance-dependent bond percolation on Delaunay triangulation networks derived from stealthy hyperuniform point configurations. The vertices of these networks correspond to the points, and the edges of the triangulation are weighted by the Euclidean distance between corresponding vertices. Since the geometric distance between points encodes crucial information about density fluctuations that is difficult to infer from purely topological network measures, such as the degree distribution [79, 80], we introduce a parameterized bond percolation model (see Sec. III, Eq. (10)) that captures Euclidean distances. In this model, low-weight edges (corresponding to nearby points) have a higher probability

of being occupied, as observed in many real-life networks. This assumption allows the model to provide insights into cluster formation in disordered systems and an emergent order on a global scale, as shown in the subsequent sections.

Weinrib and Halperin (WH) previously considered how correlated disorder in lattice systems affects percolation behaviors and the universality class [81]. In correlated percolation, the correlation of the occupation variable $\theta_i \in \{0, 1\}$ introduces disorder into block-averaged variables. In the case where θ_i follows a power-law correlation $g_\theta(r) \sim r^{-a}$, the relationship between the exponent a and the spatial dimensionality d determines the effect of the disorder [82]. Specifically, for $a < d$ the disorder decays slowly and is a relevant perturbation if $a < \frac{2}{\nu}$, whereas for $a > d$ the disorder is fast-decaying and is irrelevant if $\nu > \frac{2}{a}$; this latter property is also known as the Harris criterion [83]. In other words, disorder can shift the universality class if it is sufficiently long-ranged. The dependence of various critical exponents and scaling relations on a has been numerically studied in [84, 85]. We go beyond correlated disorder on lattices by studying networks that are not regular and using a distance-dependent bond occupation probability.

We show that adding global order to a disordered system can alter its critical behavior by determining both the critical point and the set of critical exponents for stealthy hyperuniform systems with various χ values and for the uncorrelated Poisson system. We find that under the parameterized bond percolation model, the critical point decreases with increasing degree of hyperuniformity. Our results demonstrate that stealthy hyperuniform networks can achieve global connectivity at a lower coupling scale than the uncorrelated random system.

Moreover, our results indicate that the stealthy hyperuniform systems with $\chi > 0.20$ belong to the lattice universality class, while a shift is observed for $\chi = 0.20$ and the Poisson system. We attribute this shift to the suppression of density fluctuations in the long-wavelength limit, for reasons that directly relate to the correlated disorder in the WH argument [81–83]. Therefore, we demonstrate that in addition to its structural property given by Eq. (2), hyperuniformity is also manifested as an emergent property.

These findings have multiple implications. Our results suggest that Delaunay triangulation networks derived from stealthy hyperuniform point configurations are more resilient against edge removals compared to those derived from Poisson point configurations. Furthermore, we show that the percolation threshold of stealthy hyperuniform networks is sensitive to the short-range order of the underlying point configurations, with the percolation threshold decreasing as short-range order increases. This behavior is consistent with the near-optimal conductive transport properties of high- χ stealthy hyperuniform networks observed in Ref. [69]. Lastly, the degree of stealthiness χ generates a family of stealthy hyperuniform networks with tunable critical thresholds. This provides a powerful means of probing how percolation behavior responds to controlled changes in structural correlations.

The rest of the paper is organized as follows: In Sec. II, we provide definitions of concepts associated with hyperuniformity and correlation functions. In Sec. III we introduce our parameterized bond percolation model. Section IV presents our numerical methods for studying the percolation behaviors of the stealthy hyperuniform and uncorrelated Poisson systems. In Sec. V, we present our numerical results, including the calculated values of the critical point and the critical exponents. In Sec. VI, we present concluding remarks.

II. DEFINITION OF HYPERUNIFORMITY

A point configuration in d -dimensional Euclidean space \mathbb{R}^d is completely characterized by an infinite set of n -point correlation functions $\rho_n(\mathbf{r}_1, \dots, \mathbf{r}_n)$, each of which is proportional to the probability of finding n points (representing the centers of particles) at the positions $\mathbf{r}_1, \dots, \mathbf{r}_n$ [86]. For statistically homogeneous systems, $\rho_1(\mathbf{r}_1) = \rho$, and $\rho_2(\mathbf{r}_1, \mathbf{r}_2) = \rho^2 g_2(\mathbf{r})$, where $\mathbf{r} = \mathbf{r}_1 - \mathbf{r}_2$, and $g_2(\mathbf{r})$ is the pair correlation function. If the system is also statistically isotropic, then $g_2(\mathbf{r}) = g_2(r)$, where $r = |\mathbf{r}|$. The ensemble-averaged structure factor $S(\mathbf{k})$ is defined as

$$S(\mathbf{k}) = 1 + \rho \tilde{h}(\mathbf{k}) \quad (3)$$

where $\tilde{h}(\mathbf{k})$ is the Fourier transform of the total correlation function $h(\mathbf{r}) = g_2(\mathbf{r}) - 1$, and \mathbf{k} is the wave vector.

For a single periodic point configuration with N particles at positions $\mathbf{r}^N = (\mathbf{r}_1, \dots, \mathbf{r}_N)$

within a fundamental cell F of a lattice Λ , the scattering intensity $\mathbb{S}(\mathbf{k})$ is given by

$$\mathbb{S}(\mathbf{k}) = \frac{|\sum_{j=1}^N \exp(-i\mathbf{k} \cdot \mathbf{r}_j)|^2}{N}. \quad (4)$$

In the thermodynamic limit, the scattering intensity of an ensemble of an N -particle configurations in F is related to $S(\mathbf{k})$ by

$$\lim_{N, V_F \rightarrow \infty} \langle \mathbb{S}(\mathbf{k}) \rangle = (2\pi)^d \rho \delta(\mathbf{k}) + S(\mathbf{k}), \quad (5)$$

where $\rho = N/V_F$, V_F is the volume of the fundamental cell, and δ is the Dirac delta function [1]. For finite- N simulations under periodic boundary conditions, Eq. (4) is used to compute $S(\mathbf{k})$ directly by averaging over configurations.

Consider systems characterized by a structure factor with a radial power law in the vicinity of the origin,

$$S(\mathbf{k}) \sim |\mathbf{k}|^\alpha \text{ for } |\mathbf{k}| \rightarrow 0. \quad (6)$$

The exponent α is referred to as the hyperuniformity exponent. For *hyperuniform* systems, $\alpha > 0$. A (standard) *nonhyperuniform* system has $\alpha = 0$, i.e., $S(\mathbf{k})$ approaches a non-zero constant in the zero-wavenumber limit. An *antihyperuniform* system is one possessing a diverging $S(\mathbf{k})$ in the zero-wavenumber limit, i.e., with $\alpha < 0$.

For hyperuniform systems, α determines large- R scaling behaviors of the number variance [1, 2], according to which all hyperuniform systems can be categorized into three different classes:

$$\sigma_N^2(R) \sim \begin{cases} R^{d-1} & \alpha > 1, \text{ class I} \\ R^{d-1} \ln(R) & \alpha = 1, \text{ class II} \\ R^{d-\alpha} & \alpha < 1, \text{ class III.} \end{cases} \quad (7)$$

Classes I and III are the strongest and weakest forms of hyperuniformity, respectively. Class I systems include all crystal structures [1], many quasicrystal structures [87], and certain exotic disordered systems [88, 89]. Examples of Class II systems include some quasicrystal structures [87], perfect glasses [90], and maximally random jammed packings [3–5, 91, 92]. Examples of Class III systems include classical disordered ground states [21], random organization models [11], perfect glasses [90], and perturbed lattices [93]; see Ref. [2] for a more

comprehensive list of systems that fall into the three hyperuniformity classes.

Stealthy hyperuniform systems are a special subset of class-I hyperuniform systems possessing a zero structure factor for a range of wavevectors around the origin, i.e.,

$$S(\mathbf{k}) = 0, \quad \text{for } \mathbf{k} \in \Omega, \quad (8)$$

excluding the forward scattering. Stealthy hyperuniform systems include all crystals, most quasicrystals and certain special disordered systems [2]. The degree of stealthiness and short-range order in the system is determined by a tuning parameter χ measuring the fraction of the independently constrained degrees of freedom M within the exclusion region Ω (i.e., half the number of \mathbf{k} points in Ω) [22, 27, 28, 94], i.e.,

$$\chi = \frac{M}{(N-1)d} \quad (9)$$

where N is the total number of points in the systems. We note that d degrees of freedom associated with the trivial overall translation of the entire system are subtracted in Eq. (9). Stealthy hyperuniform systems distinguish themselves from standard hyperuniform systems in that they completely suppress density fluctuations at the intermediate to infinite wavelengths. In contrast, standard hyperuniform systems only completely suppress infinite-wavelength density fluctuations.

III. PARAMETERIZED BOND PERCOLATION MODEL

Consider a Delaunay triangulation graph G corresponding to a point configuration, in which each edge is weighted by the Euclidean distance between the two connected vertices. We propose the following bond percolation model: in G , each edge $e_{ij} \in E(G)$ is retained independently with probability

$$p_{ij} = \max\left(0, 1 - \frac{d_{ij}}{z}\right) \quad (10)$$

where d_{ij} is the Euclidean distance between two connected vertices i and j , and z is the tuning parameter that plays a role analogous to temperature in the Ising model or the oc-

cupation probability p in Bernoulli percolation. In other words, each edge has a probability $1-p_{ij} = \min\left(1, \frac{d_{ij}}{z}\right)$ of being absent. This model reflects the physical assumption that longer edges are less likely to be present. Indeed, interactions limited by distance are observed in many real-life networks, including epidemic contact networks and neuronal signaling [95–98].

Effectively, we map distances between vertices onto an interaction network, where edge presence is governed by the distance-dependent probability p_{ij} . The interaction probabilities satisfy the relationship $\frac{1-p_{ij}}{1-p_{mn}} = \frac{d_{ij}}{d_{mn}}$ for $z > d_{ij}, d_{mn}$, which shows that the interactions strengths preserve the spatial correlations in the point configurations. The parameter z sets the global scale of the interaction strength. In the limit $z \rightarrow 0$, there are no edges in the network. In the limit $z \rightarrow \infty$ all the edges of the Delaunay triangulation are present. There is a phase transition at some finite z_c above which a percolating cluster is observed.

IV. METHODS

We determine the critical point z_c and the corresponding set of critical exponents for the stealthy hyperuniform networks with various χ values as well as for the Poisson networks using Monte Carlo simulations and finite-size scaling.

A. Generation of hyperuniform networks

Disordered stealthy hyperuniform point configurations investigated in this work are generated using the so-called “collective coordinates” approach [24, 27, 28]. Starting from a random initial configuration, the positions of the points are randomly perturbed to minimize the difference between the system’s structure factor and the targeted structure factor within the exclusion region $\mathbf{k} \in \Omega$, via stochastic optimization. In this work, we include stealthy hyperuniform systems with $\chi = 0.20, 0.40$ and 0.49 .

To perform finite-size scaling, as described in Sec. IV B, it is necessary to generate systems of different linear sizes. For a linear size L , $N = L^2$ points are generated in an $L \times L$ box. Due to the stochastic nature of the point configurations, we prepare $N_{real} = 20$ disordered realizations for each linear size to compute ensemble-averaged observables. To balance the

computational cost of system generation with the need for high statistics in the percolation calculations, we study linear sizes in the range $20 \leq L \leq 200$.

Once the stealthy hyperuniform point configurations are obtained, we construct networks (or graphs) via Delaunay triangulation with periodic boundary conditions, following Ref. [72, 80]. In a Delaunay triangulation of a point configuration, the points become vertices of the graph, and edges are drawn between neighboring points such that the resulting graph is planar, triangular, and the circumcircles of each triangle do not contain any other points. Figure 1 illustrates the structure of the Delaunay triangulation of the three stealthy hyperuniform systems, as well as the Delaunay triangulation of an uncorrelated Poisson point configuration.

B. Finite-size scaling

Phase transitions are associated with non-analytic behaviors in thermodynamic quantities. Such behaviors cannot arise in finite systems, where all thermodynamic functions are analytic. A naive fitting near the critical point in a finite system would lead to significant inaccuracies. Instead, finite-size scaling compares the correlation length ξ with the linear size L of the system to study how thermodynamic variables scale as functions of L [99]. An observable $Q(z) \sim |z - z_c|^{-q}$ in the thermodynamic limit scales as

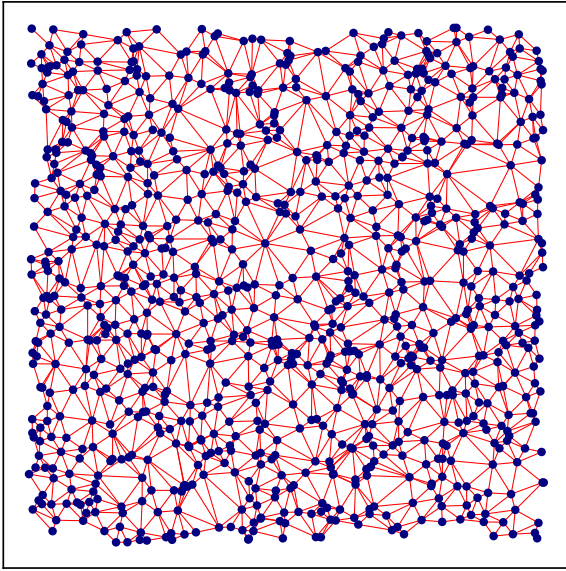
$$Q_L(z) = L^{\frac{q}{\nu}} F(x) \quad (11)$$

when the system is finite, where $F(\cdot)$ is some scaling function and $x = (z - z_c)L^{\frac{1}{\nu}}$. In particular, the probability that there exists a percolating cluster, $R_L(z)$, scales as

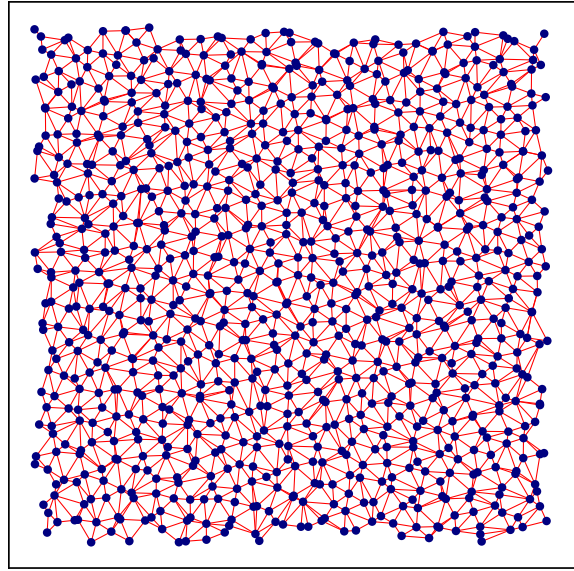
$$R_L(z) = \Phi(x) \quad (12)$$

which becomes a step function centered at z_c as $L \rightarrow \infty$. $R_L(z)$ plays a central role in determining the critical point z_c and the exponent ν . Knowing the value of the exponent ν allows the calculation of many other exponent q since $Q_L(z_c) \propto L^{\frac{q}{\nu}}$.

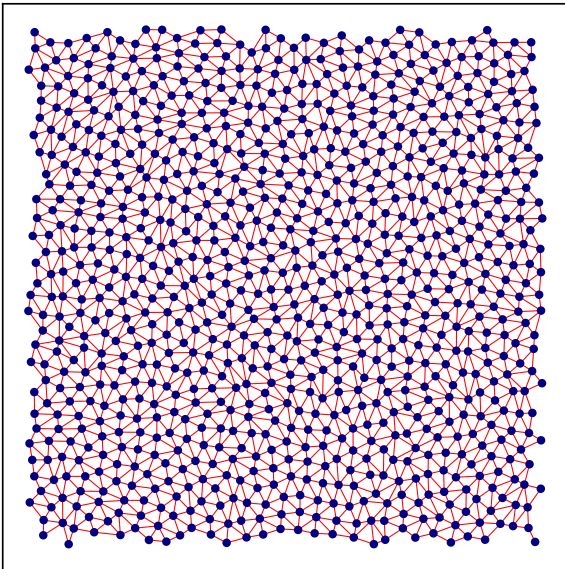
First, ν can be calculated by noting that if one defines two constants R_1 and R_2 such



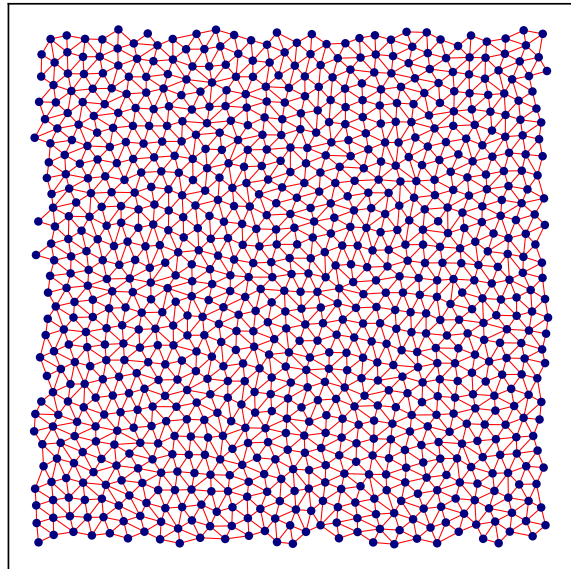
(a) Poisson



(b) Stealthy hyperuniform $\chi = 0.20$



(c) Stealthy hyperuniform $\chi = 0.40$



(d) Stealthy hyperuniform $\chi = 0.49$

FIG. 1. Delaunay triangulation of Poisson and stealthy hyperuniform point configurations. The vertices are shown as dark blue points, and edges are shown in red. Only a section of the periodic network (toroidal topology) is displayed for visual representation.

that $R_L(z_1) = R_1$ and $R_L(z_2) = R_2$, Eq. (12) suggests that the width $\Delta z = z_1 - z_2$ scales as

$$\Delta z \propto L^{-\frac{1}{\nu}} \quad (13)$$

The scaling relation is independent of the choice of R_1 and R_2 , which only affects the prefactor. Intuitively, this scaling relation can also be understood by noting that the correlation length $\xi \sim |z - z_c|^{-\nu}$ becomes comparable to L at the critical point, which implies $|z - z_c| \sim L^{-\frac{1}{\nu}}$. Therefore, the critical exponent ν can be evaluated with Eq. (13) by calculating Δz for different L .

Second, z_c is determined by making the observation that

$$\frac{dR_L(z)}{dz} = L^{\frac{1}{\nu}} \Phi'(x) \quad (14)$$

We define a pseudocritical point $z_c(L)$ where the slope $\frac{dR_L(z)}{dz}$ is maximal. According to Eq. (14), this occurs at $x^* = (z_c(L) - z_c) L^{\frac{1}{\nu}}$ where x^* is a constant, and therefore,

$$z_c(L) = z_c + x^* L^{-\frac{1}{\nu}} \quad (15)$$

Along with Eq. (13), z_c can be determined as

$$z_c(L) - z_c \propto \Delta z \quad (16)$$

In particular, Yonezawa et al. proposed that $\frac{dR_L(z)}{dz}$ takes the form of a Gaussian function [100]

$$\frac{dR_L(z)}{dz} = A \exp \left\{ -\frac{1}{2} \left(\frac{z - z_c(L)}{\sigma} \right)^2 \right\} \quad (17)$$

We compute $R_L(z)$ with the Newman-Ziff algorithm, from which z_c and ν were determined.

C. Simulation with the Newman-Ziff algorithm

The Newman-Ziff algorithm is a fast Monte Carlo simulation first proposed to determine the critical point of Bernoulli percolation in lattices [101]. Instead of directly sampling configurations at various probabilities p , the algorithm starts from an empty initial configuration and scans through p by sequentially adding bonds. The major speed-up comes from the use of the Union-Find data structure, which stores all cluster information in rooted trees.

Constructing configurations for our non-uniform percolation model is more involved than for Bernoulli percolation. For each run, we generate a random number $u_{ij} \sim \mathcal{U}(0, 1)$ for each edge e_{ij} , which is then assigned a corresponding threshold $z_{ij} = \frac{d_{ij}}{1-u_{ij}}$. We then sort the edges in the ascending order of z_{ij} . For a given grid of z values, the configuration at each z includes all edges with $z_{ij} \leq z$. This is equivalent to sampling the occupation probability p_{ij} , since

$$p_{ij} = \mathbb{P}\left(u_{ij} \leq 1 - \frac{d_{ij}}{z}\right) = \mathbb{P}(z_{ij} \leq z) \quad (18)$$

In a finite system, a percolating cluster can be defined in various ways. Under open boundary conditions, it is often defined as the cluster that spans from the top to the bottom or from the left to the right boundaries of the system. Alternatively, under periodic boundary conditions, a percolating cluster can be defined as one that wraps around the torus. It has been demonstrated that simulations of the percolation threshold converge more rapidly under periodic boundary conditions due to the reduced boundary effects [101].

We simulate the wrapping probability (i.e., the probability that a percolating cluster exists) $R_L(z)$ on the torus to determine the critical point z_c . In the simulation, we add edges sequentially in ascending order of z_{ij} and check wrapping at each step. First of all, wrapping requires the formation of a non-contractible loop on the torus, which only occurs when a newly added edge connects two vertices that already belong to the same cluster. To further check whether the newly added edge results in a wrapping, we build upon the method used in continuum percolation [102]. Whenever we use Union-Find to identify the root of a vertex k , we calculate the displacement \vec{d}_k from k to its root under periodic boundary conditions. When an edge e_{ij} is added and i and j already share the same root, we calculate the loop displacement \vec{D}_{loop} from i to the root, the root to j , and j to i :

$$\vec{D}_{loop} = \vec{d}_i - \vec{d}_j + \Delta\vec{r}_{ij} \quad (19)$$

where $\Delta\vec{r}_{ij}$ is the displacement from j to i under periodic boundary condition. This gives

the winding number of the cluster to which i and j belong in both the x and y directions:

$$n_m = \frac{D_{loop}^m}{L}, \quad m = x, y \quad (20)$$

n_m is a non-zero integer if wrapping in the m direction is induced by the edge e_{ij} . Otherwise, $\vec{D}_{loop} = 0$ and $n_m = 0$. Once percolation has occurred, adding more edges, hence higher z , will always give a wrapping configuration. The algorithm can therefore be stopped after detecting wrapping for the first time.

For each realization i of the disordered system, we repeat the run N times and record the number of runs N_{wrap} in which wrapping has occurred. This gives the wrapping probability $R_L^i(z) = \frac{N_{wrap}}{N}$ for realization i . The ensemble average $\langle R_L(z) \rangle$ is then

$$\langle R_L(z) \rangle = \frac{1}{N_{real}} \sum_i R_L^i(z) \quad (21)$$

where N_{real} is the number of disordered realizations. In particular, we study both horizontal and vertical wrapping; their average, as shown by Yonezawa et al. [100], gives the true wrapping probability. We generated $N_{real} = 20$ for each linear size L , and for each disordered realization, we ran the simulation 10^6 times for $L \leq 40$ and 10^5 times for $L > 40$.

D. Data collapse optimization

For a phase transition model that obeys finite-size scaling [see Eq. (12)], $\langle R_L(z) \rangle$ for different L are expected to collapse onto a single scaling function $\Phi(x)$ when plotted against $x = (z - z_c)L^{\frac{1}{\nu}}$ with the true z_c and ν of the system. Thus, data collapse serves as a consistency check of the finite-size scaling ansatz and of the estimated z_c and ν .

We refine the initial estimate of z_c from Eq. (16) and (17) via a one-dimensional optimization of a collapse cost. We define a grid of $\{x_i = (z_i - z_c)L^{\frac{1}{\nu}}\}$ values in the critical region, from which $R_L(x_i)$ could be calculated for all L . The collapse error is then defined to be the summed variance of $R_L(x_i)$ across different linear sizes, and is minimized with respect to z_c in the vicinity of the previously estimated value. We keep ν fixed because

its finite-size scaling estimate given by Eq. (13) is stable and low-variance, as detailed in Sec. V A. We estimate uncertainties via bootstrap resampling of realizations, and report the mean and standard deviation of the bootstrap z_c estimates. The refined z_c values yield a stronger collapse onto a single universal scaling function, as shown in Sec. V A.

V. RESULTS

We use the Newman-Ziff algorithm as described in Sec. IV to first determine the average wrapping probability $\langle R_L(z) \rangle$, from which we estimate the critical point z_c . We then calculate the critical exponents ν , γ , τ as well as the fractal dimension d_f to characterize the universality class of the systems.

A. The critical point

The wrapping probability for each individual realization R_L^i is first smoothed by a Savitzky-Golay filter, then numerically differentiated to give $\frac{d\langle R_L(z) \rangle}{dz}$. Figure 2 shows the derivatives $\frac{d\langle R_L(z) \rangle}{dz}$ for $L = 20, 50$ and 100 along with their Gaussian fits. The derivatives are smooth on the grid of z values, which strongly suggests that $\langle R_L(z) \rangle$ has converged. The pseudocritical point $z_c(L)$ is then determined with Eq. (17). The Gaussian fit of $\frac{d\langle R_L(z) \rangle}{dz}$ assumes an antisymmetric $\langle R_L(z) \rangle$, and provided a reasonable fit for large linear sizes L , yielding the pseudocritical points shown with blue \times symbols in Fig. 2. However, the fit exhibits noticeable discrepancies at small L . Instead of the Gaussian fit, we applied a quadratic fit in the vicinity of the absolute maximum on the z -grid to find the true $z_c(L)$; these values are shown as red \times symbols. A quadratic fit is possible because of the smoothness of the data points due to the high statistics. We generate $N = 10^4$ bootstrap samples by resampling the set of realizations of $\frac{d\langle R_L(z) \rangle}{dz}$ with replacement.

We then determine the width of the transition Δz . In theory, the calculations of z_c and ν are independent of the choice of R_1 and R_2 that define Δz , as shown in Sec. IV B. Numerically, close to the transition, i.e., at $R_1, R_2 \sim 0.5$, the fluctuations are large, leading to large uncertainties in Δz . The error bars in Δz were estimated from the cross-realization fluctuations when solving for $R_L(z_i) = R_i$ where $i = 1, 2$. We choose $R_1 = 0.85$ and $R_2 = 0.15$

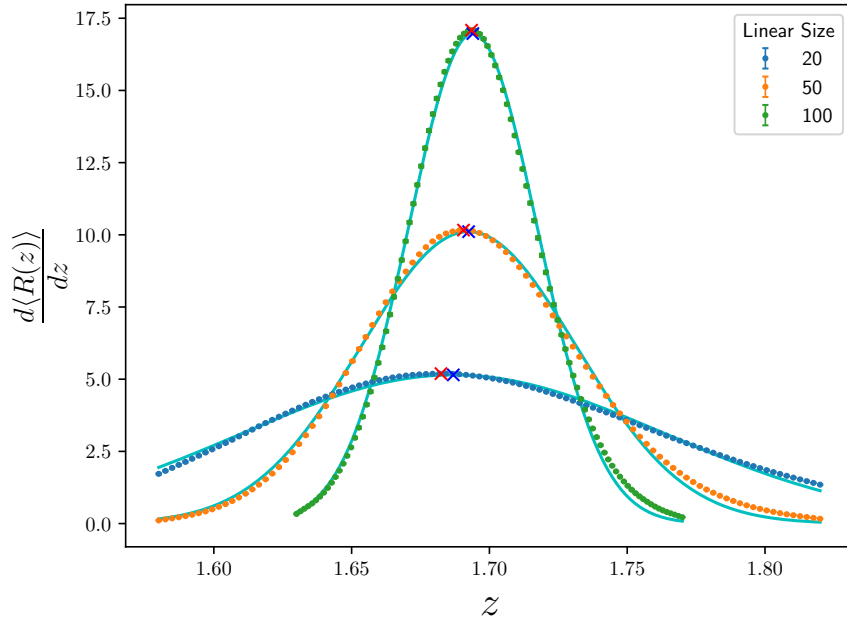


FIG. 2. The derivative of the wrapping probability, $\frac{d\langle R_L(z) \rangle}{dz}$, of stealthy hyperuniform systems with $\chi = 0.49$ for $L = 20, 50$ and 100 . The error bars on the mean have two sources: (a) intrasample variation, arising from the binomial uncertainty within each realization (negligible in this case due to the large number of runs), and (b) intersample variation, arising from fluctuations across independent realizations, which dominate the reported error bars. The pseudocritical points $z_c(L)$ estimated from Gaussian fitting are marked by blue \times , whereas quadratic fits near absolute maxima yield estimates marked as red \times . The difference between the two estimates decreases with increasing linear size.

to ensure that the errors associated with Δz are small, while the transition width is still defined within the critical region. Notably, the values of z_c and ν obtained using different choices of R_1 and R_2 remained consistent within the error bars. With $z_c(L)$ and Δz , the critical point in the thermodynamic limit can be determined from Eq. (16). Figure 3 shows the finite-size scaling of $z_c(L)$ across all four systems, highlighting a clear hierarchy: the more ordered the system, the lower its critical point.

The critical exponent ν is obtained from the slope of $\ln \Delta z$ versus $\ln L$, as given by Eq. (13). Figure 4 shows the scaling results for all four systems. For visual comparison of the slopes, the data points are vertically shifted by aligning the values at $L = 20$. In addition, the theoretical scaling of $\ln \Delta z$ predicted for the lattice universality class ($\nu = \frac{4}{3}$) is plotted as a reference line. The stealthy hyperuniform systems with $\chi = 0.40$ and 0.49 exhibit a strong agreement with the lattice universality class value $\nu = 4/3$, while the Poisson

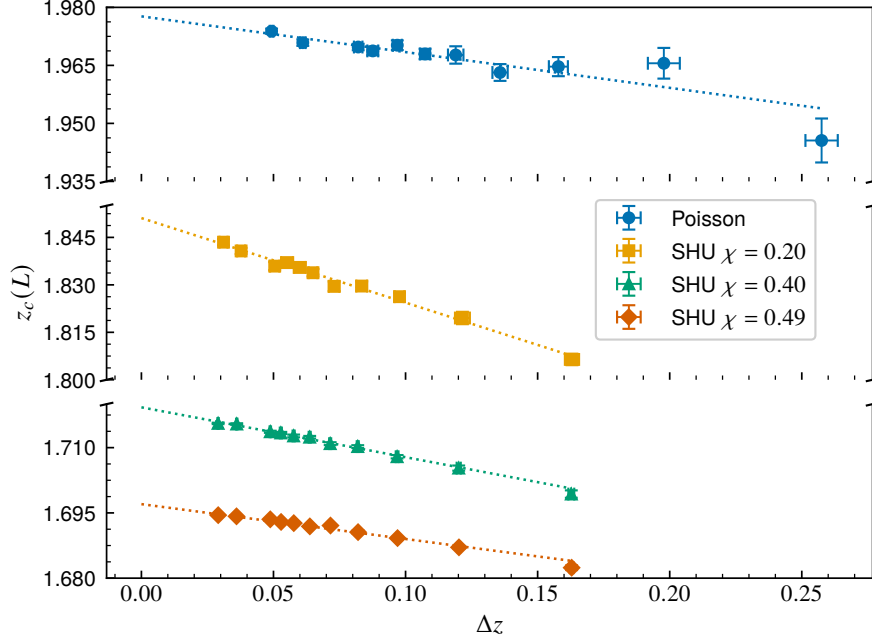


FIG. 3. Extrapolation of the pseudocritical point $z_c(L)$ to the thermodynamic limit ($\Delta z \rightarrow 0$) for all systems. The more ordered systems are found to have a lower critical point. The uncertainties in Δz reflect the cross-realization fluctuations of the crossing points z_1 and z_2 . The uncertainties in $z_c(L)$ and Δz decrease with the linear size L .

and $\chi = 0.20$ systems deviate with increasing L , suggesting differences in ν . This deviation may indicate a shift in the universality class, an interesting phenomenon further examined in Sec. VB. The good agreement between the data points and the fits demonstrates robust convergence of the exponent estimates.

We assess the accuracy of the estimates of z_c and ν by performing data collapse, i.e., checking whether the average wrapping probabilities $\langle R_L(z) \rangle$ for all linear sizes L collapse onto a single universal scaling function. Figure 5 shows the data collapse of the stealthy hyperuniform systems with $\chi = 0.49$. As seen in Fig. 5, the estimated z_c and ν yield a reasonable collapse, but with a small misalignment. This is because the data collapse is very sensitive to z_c , whose estimation suffered from the noise, especially at small L , due to uncertainties in both Δz and $z_c(L)$ [see Fig. 3]. To improve the estimation of z_c , we employ the optimization algorithm detailed in Sec. IVD. After optimization, the wrapping probabilities $\langle R_L(z) \rangle$ exhibit a stronger collapse onto a single function as shown in Fig. 5b.

Table I summarizes the calculated z_c and ν for all systems. We find that the stealthy hyperuniform networks exhibit a lower critical point z_c than that of an uncorrelated random

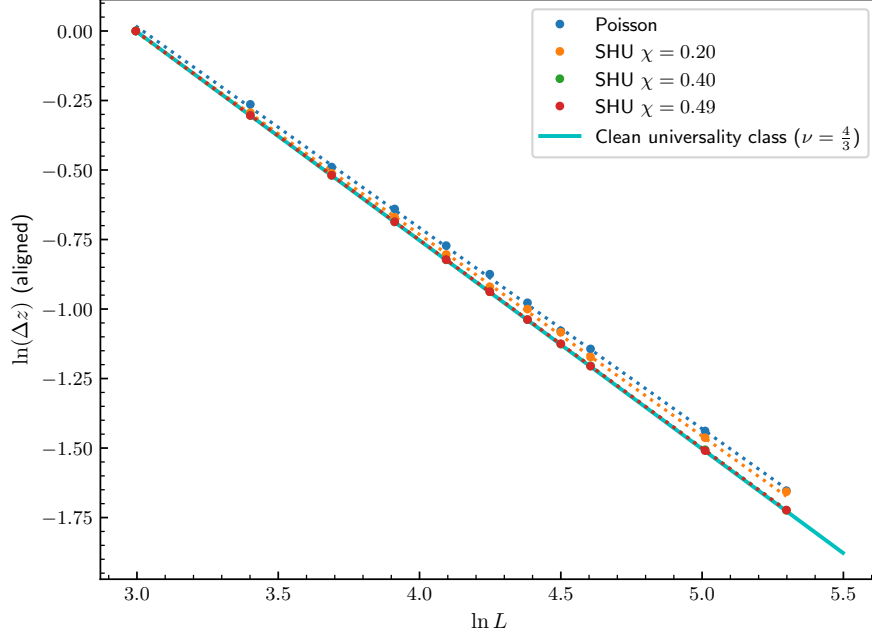


FIG. 4. Finite-size scaling of the transition width for all systems. Data points are vertically shifted so that the values at $L = 20$ coincide. The expected scaling for the lattice universality class ($\nu = \frac{4}{3}$) is shown in cyan for comparison. The linear fits exhibit excellent convergence, supporting the robustness of the critical exponent ν estimates. Stealthy hyperuniform (SHU) systems with $\chi = 0.49$ and $\chi = 0.40$ show strong agreement with the lattice (clean) universality class value, while SHU with $\chi = 0.20$ and Poisson exhibit deviations.

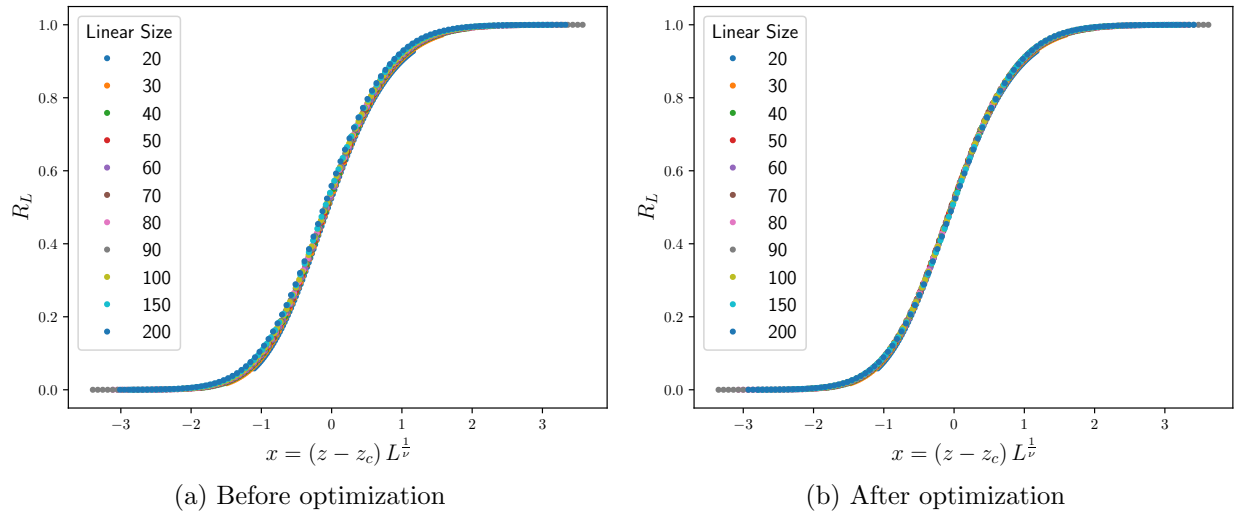


FIG. 5. The data collapse of stealthy hyperuniform systems with $\chi = 0.49$ is shown (a) before and (b) after applying the optimization algorithm described in Sec. IV D. In (a), the collapse exhibits a small but visible misalignment, reflecting a deviation from the true z_c . After optimization (b), the collapse improves significantly, producing a more accurate estimate of z_c .

network, $z_c^{\text{SHU}} < z_c^{\text{Poi}}$. This means that stealthy hyperuniform networks can achieve global connectivity at a lower coupling scale than the uncorrelated random network. We propose that this hierarchy of critical points is a direct consequence of the suppression of density fluctuations in the underlying stealthy hyperuniform point configurations.

Figure 6 supports this interpretation by showing configurations for Poisson and stealthy hyperuniform ($\chi = 0.40$) systems at an intermediate value $z^* = 1.8$ such that $z_c^{\text{SHU}} < z^* < z_c^{\text{Poi}}$. Due to the distance dependence of the bond occupation probability, nearby sites are connected first as the coupling scale z increases. For the Poisson system, this mechanism leads to highly localized clusters surrounded by sizable voids, and to achieve global connectivity, a higher coupling scale is required to bridge the gaps between local clusters. Conversely, stealthy hyperuniformity suppresses such microclustering, which shortens the required bridge lengths and yields a lower critical point. In particular, it has been shown that disordered stealthy configurations across the first three space dimensions possess “bounded holes” in the infinite-system-size limit, in contrast to Poisson systems which can possess arbitrary large holes [94]. Moreover, previous studies on continuum percolation of two-phase media similarly observed that large holes are heavily suppressed in stealthy hyperuniform systems, leading to decreased percolation thresholds in such systems [64]. Our results demonstrate that a similar suppression mechanism lowers the percolation threshold in stealthy hyperuniform networks, indicating that the enhanced percolation properties of stealthy hyperuniform systems extend beyond the continuum model shown in Ref. [64].

TABLE I. The critical point z_c and the critical exponent ν of the uncorrelated (Poisson) and the stealthy hyperuniform networks with different χ values.

Systems	z_c	ν
Poisson	1.97432 ± 0.00078	1.38300 ± 0.01786
Stealthy $\chi = 0.20$	1.85012 ± 0.00118	1.37868 ± 0.02435
Stealthy $\chi = 0.40$	1.71752 ± 0.00019	1.33691 ± 0.00574
Stealthy $\chi = 0.49$	1.69540 ± 0.00009	1.33572 ± 0.00295

Interestingly, the critical point of stealthy hyperuniform networks could be controlled by varying the stealthiness parameter χ : the higher the χ value, the lower the critical point. This behavior arises because χ directly controls the degree of short-range order in the system, and microclustering is highly suppressed when all edges have comparable

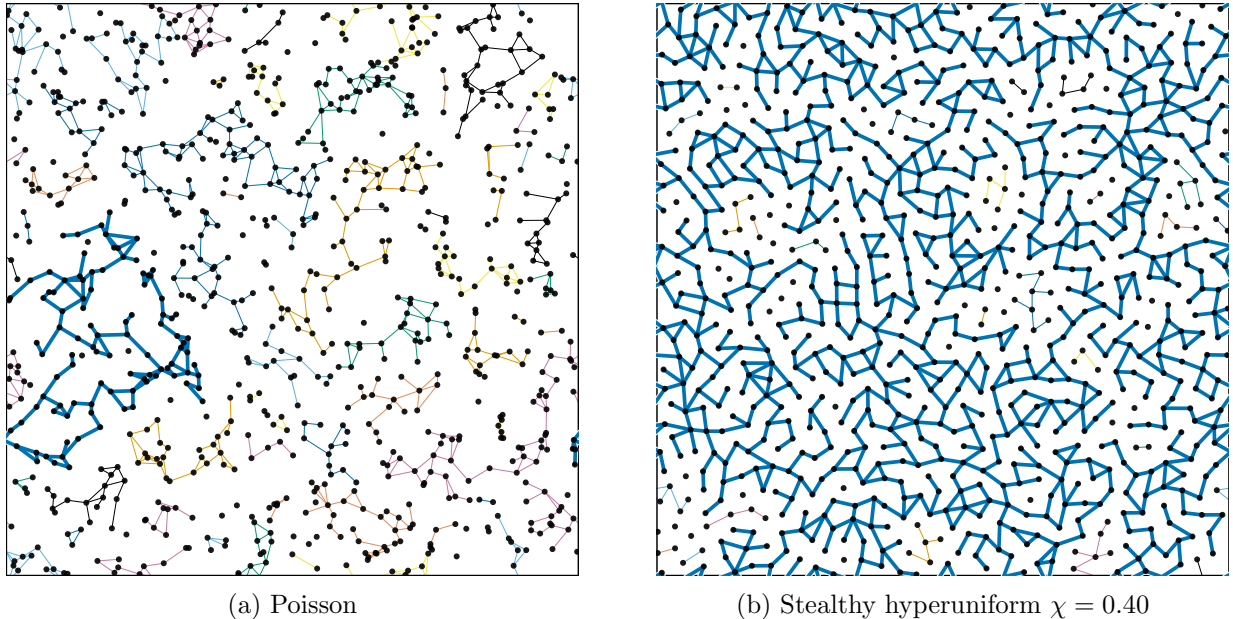


FIG. 6. Configurations of (a) Poisson and (b) stealthy hyperuniform ($\chi = 0.40$) systems at $z^* = 1.8$, which lies between the critical points of the two systems under the percolation model given by Eq. 10. The system size is 30×30 for both systems, with periodic boundary conditions. Disjoint clusters are denoted by different colors. The largest cluster is highlighted with thick blue bonds. The Poisson configuration exhibits pronounced microclustering, which is strongly suppressed in the hyperuniform case.

occupation probability, as it is the case for systems with pronounced local order. The non-universal percolation threshold z_c is sensitive to such microscopic structural details. Therefore, stealthy hyperuniformity enables controlled manipulation of network criticality through structural correlations, offering new opportunities for optimizing connectivity in disordered systems.

B. Critical exponents and universality class

To investigate the universality class of the systems, we calculate their corresponding set of critical exponents. The fractal dimension d_f characterizes how the mass $M(L)$ of the percolating cluster at criticality scales with the linear size L , i.e., $M(L) \sim L^{d_f}$. The critical exponent γ characterizes the divergence of the mean cluster size, excluding the percolating cluster, near z_c , i.e., $S(z) = \sum s^2 n_s \sim |z - z_c|^{-\gamma}$ where n_s is the number density of finite (non-percolating) clusters of size s . The exponent γ can be determined at $z = z_c$ from the equation $\ln S_L(z_c) = \frac{\gamma}{\nu} \ln L + C$ where C is some constant. Scaling theory also predicts that

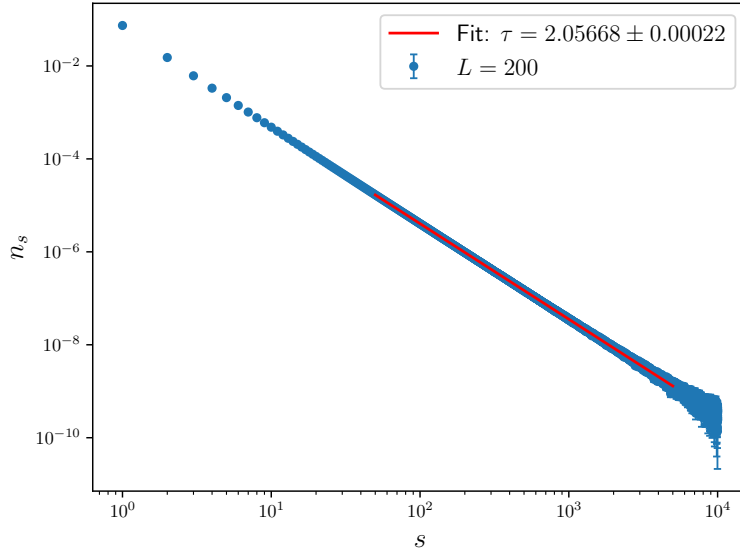


FIG. 7. Cluster statistics n_s of stealthy hyperuniform networks ($\chi = 0.49$) with linear size $L = 200$ at the estimated critical point z_c . Data are truncated at $s = 10000$ to avoid finite-size noise. The power-law fit over $s \in [50, 5000]$ excludes discreteness at small s and finite-size effects at large s . The observed power-law scaling of n_s supports the accuracy of our z_c estimate.

$n_s(z) = q_0 s^{-\tau} f[q_1(z - z_c)s^\sigma]$. The power law distribution of cluster sizes $n_s \sim s^{-\tau}$ at the critical point defines the exponent τ .

We perform direct sampling of the clusters at $z = z_c$ to calculate d_f , γ , and τ . For each configuration, we calculate n_s and $M(L)$, from which $S_L(z_c)$ can be recovered. The simulation is run 10^6 times for $L \leq 40$ and 10^5 times for $L > 40$ for all 20 disordered realizations of all systems.

In practice, the power law distribution of the cluster statistics $n_s \sim s^{-\tau}$ holds only for intermediate s . Figure 7 shows the cluster statistics of the stealthy system with $\chi = 0.49$ at criticality. When calculating τ , we introduce cutoffs s_{\min} and s_{\max} to exclude the small- s discreteness effects and the large- s finite-size cutoff. Although τ can in principle be estimated at any linear size L , we report the values from the largest system available ($L = 200$) to minimize the finite-size effects and maximize the scaling window ($s_{\max} - s_{\min}$).

The cluster-size distribution exhibits a clear power-law regime over an intermediate range, and the numerical value of τ is stable against variations of s_{\min} and s_{\max} . This is consistent

with the system being at criticality and supports the accuracy of our estimated z_c . The numerical results for d_f , γ , and τ are summarized in Table II. We note that extracting τ with the same level of confidence as the others is more challenging due to finite-size effects.

TABLE II. The obtained values of the fractal dimension d_f and the critical exponents γ , τ for the four systems.

Systems	d_f	γ	τ
Poisson	1.89554 ± 0.00250	2.50453 ± 0.03415	2.03833 ± 0.00039
Stealthy $\chi = 0.20$	1.90901 ± 0.00326	2.45959 ± 0.04516	2.13197 ± 0.00076
Stealthy $\chi = 0.40$	1.89714 ± 0.00090	2.40136 ± 0.01052	2.07083 ± 0.00029
Stealthy $\chi = 0.49$	1.89589 ± 0.00048	2.39830 ± 0.00540	2.05668 ± 0.00022

The fractal dimension of all four systems agrees with the lattice universality class value, which is $d_f = \frac{91}{48} \approx 1.89583$. In contrast, the systems differ in the degree of agreement of their ν (see Table I) and γ values with the lattice values of $\nu = \frac{4}{3}$ and $\gamma = \frac{43}{18} \approx 2.38889$. The stealthy systems with $\chi \geq 0.40$ remain consistent with the lattice universality class, whereas the $\chi = 0.20$ stealthy system and the Poisson system display small but noticeable shifts from it. This is also illustrated in Fig. 4. A shift in the critical exponent ν , while the fractal dimension d_f remains at its lattice universality class value, has also been observed in numerical studies of correlated percolation where $g_\theta(r) \sim r^{-a}$ [84, 85]. These studies found that in 2D, the exponent ν begins to deviate from its lattice universality class value and shifts to $\nu_{\text{corr}} = \frac{2}{a}$ when $a < \frac{3}{2}$, as predicted by the WH criterion, whereas changes in d_f , τ , and in ratios of critical exponents such as $\frac{\gamma}{\nu}$ occur only for even longer-range correlations, i.e., when $a < \frac{2}{3}$.

Our observed deviation of the Poisson system's value for certain critical exponents highlights that hyperuniformity plays a significant role in shaping the universality class of disordered systems. To assess the stability of a lattice critical point against quenched disorder, Harris and subsequently Weinrib and Halperin introduced the idea of examining the variance of the block-averaged control parameter (e.g., the local density) over regions of linear size ξ_V [81–83]. The relevance of disorder is then governed by how the variance of the block-averaged local parameter decreases as the correlation length grows when approaching the critical point. From this perspective, it is expected that high- χ stealthy hyperuniform point configurations, which strongly suppress large-scale density fluctuations, remain in the

lattice universality class since the variance of their block-averaged disorder (e.g., density variance) decays sufficiently rapidly as the correlation length diverges.

In contrast, Poisson configurations generate pronounced local density fluctuations, which translate into clusters of anomalously short edges in the Delaunay triangulation network, as can be seen in Fig. 1. It was also shown previously that stealthy hyperuniform configurations with $\chi \leq 0.30$ can have points arbitrarily close to each other [64], leading to such clustering in the stealthy systems with $\chi = 0.20$, though to a lesser degree. Because our bond-occupation probability depends on edge length, these short-edge clusters are preferentially occupied, effectively amplifying disorder correlations. This is illustrated in Fig. 6. Under coarse-graining, this drives the block-averaged control parameter to a different fixed point, consistent with a shift in universality class.

This interpretation is in agreement with a recent study by Mitra, Mukherjee and Mohanty [103], wherein hyperuniform point configurations are generated by energy thresholding of the critical Ashkin-Teller model on square lattices. Hyperuniform point configurations are found to remain in the lattice universality class, whereas increasing long-wavelength density fluctuations drive a continuous shift of the universality classes, reflected in smoothly varying critical exponents. The problem setup of Mitra et al is different from ours: hyperuniformity is a property of the underlying scalar field and thus of the thresholded occupancy in their work, while we analyze bond percolation on Delaunay-triangulated graphs of hyperuniform point configurations. Our simulations indicate that the onset of a universality-class shift emerges around $\chi \lesssim 0.20$. We attribute this shift to the point-set-to-graph mapping, which imposes stringent geometric constraints and induces correlated bond disorder. Indeed, there is growing interest in how faithfully different network constructions preserve the structural information of the underlying point configuration [79, 80, 104], as we will discuss in Sec. VI.

VI. CONCLUSION & DISCUSSION

In this work, we examine the percolation properties of Delaunay triangulation networks derived from stealthy hyperuniform point configurations with various χ under a

distance-dependent bond-percolation model (Eq. (10)) that mirrors the structure of numerous empirical spatial networks. We also include Poisson point configurations in our study for comparison. We extend the classical Newman-Ziff algorithm to non-Bernoulli percolation problems via Eq. (18). Our results show that the critical point z_c depends strongly on the degree of hyperuniformity of the spatial embeddings, and increasing the short-range order gives rise to a lower critical point. The lower percolation thresholds observed in stealthy systems are also closely linked to their “bounded-hole” property. Specifically, disordered stealthy configurations in one, two, and three dimensions possess bounded holes in the infinite-system-size limit, in contrast to Poisson systems which can possess arbitrary large holes due to unbounded void fluctuations [94]. Moreover, the critical exponents ν and γ are functions of the degree of hyperuniformity, whereas the fractal dimension d_f remains at its lattice value. Thus, it is the large-scale density fluctuations that act as the relevant perturbation in the WH sense, and increasing hyperuniformity renders the disorder irrelevant, which stabilizes the clean fixed point.

We mainly focus on the critical behavior of networks derived from spatial point configurations using the Delaunay triangulation, which is a natural baseline due to its parameter-free nature, generality, and its ability to capture local geometry. Nonetheless, as noted in [80, 104], the graph representation inevitably discards certain aspects of the underlying spatial structure, and other network constructions may lead to different effective disorder correlations. Delaunay triangulation yields a planar embedding (toroidal under PBC), enabling straightforward topological detection of wrapping and straightforward finite-size-scaling analyses. By contrast, many alternative spatial network constructions often produce non-planar graphs, complicating wrapping diagnostics and finite-size scaling studies. In those cases, the generating function formalism proposed in [75, 105] might be more suitable. It would be interesting to further study the impact of network topology on their critical behavior in the future.

Our results have several important implications. First, stealthy hyperuniform networks exhibit long-range connectivity at lower global coupling scale. Since diffusion in disordered media can be modeled as a random walk on percolation clusters, the emergence of a spanning cluster is essential for long-range diffusion [99]. The reduced connectivity threshold

of stealthy hyperuniform networks implies that system-spanning connectivity forms more readily in them than in Poisson systems. Therefore, stealthy hyperuniformity promotes the structural conditions necessary for efficient transport in discrete networks, in agreement with prior studies of transport in both continuum two-phase media [64] and cellular networks [69].

Furthermore, our findings open up the possibility of optimizing the resilience of disordered planar networks that are statistically homogeneous and isotropic. Percolation has been used to model network resilience such as random breakdowns of the Internet [75, 76]. A network is considered resilient if random removal of a large fraction of vertices or edges does not lead to fragmentation of the spanning cluster. In our model, the edge removal is distance-dependent and a resilient network corresponds to one with a low critical point, i.e., when most edges are removed. Hence, hyperuniform-based Delaunay networks are more resistant to distance-dependent edge removal than those built from uncorrelated point configurations.

More importantly, we identify stealthy hyperuniformity as an emergent property that manifests from macroscopic critical behavior. This reframes stealthy hyperuniformity as a property diagnosable from phase-transition observables rather than only from structure factors. Therefore, stealthy hyperuniform disorder provides a compelling avenue for studying critical phenomena and a systematic way to tune network criticality. Lastly, we show that network methods extend naturally to physical systems, including the disordered materials studied in this paper, enabling quantitative analysis of their critical behavior.

In future work, we will investigate the percolation behavior of other disordered systems with “bounded holes,” such as random sequential addition (RSA) packings [106, 107]. We hypothesize that these systems will exhibit lower percolation thresholds than the corresponding Poisson system, owing to their enhanced short-range order and suppressed large void fluctuations.

ACKNOWLEDGMENTS

This work was supported by the Army Research Office under Cooperative Agreement Number W911NF-22-2-0103.

- [1] S. Torquato and F. H. Stillinger, *Phys. Rev. E* **68**, 041113 (2003).
- [2] S. Torquato, *Phys. Rep.* **745**, 1 (2018).
- [3] A. Donev, F. H. Stillinger, and S. Torquato, *Phys. Rev. Lett.* **95**, 090604 (2005).
- [4] C. E. Zachary, Y. Jiao, and S. Torquato, *Phys. Rev. Lett.* **106**, 178001 (2011).
- [5] Y. Jiao and S. Torquato, *Phys. Rev. E* **84**, 041309 (2011).
- [6] D. Chen, Y. Jiao, and S. Torquato, *The Journal of Physical Chemistry B* **118**, 7981 (2014).
- [7] L. Berthier, P. Chaudhuri, C. Coulais, O. Dauchot, and P. Sollich, *Phys. Rev. Lett.* **106**, 120601 (2011).
- [8] R. Kurita and E. R. Weeks, *Phys. Rev. E* **84**, 030401 (2011).
- [9] G. L. Hunter and E. R. Weeks, *Reports on progress in physics* **75**, 066501 (2012).
- [10] R. Dreyfus, Y. Xu, T. Still, L. A. Hough, A. G. Yodh, and S. Torquato, *Phys. Rev. E* **91**, 012302 (2015).
- [11] D. Hexner and D. Levine, *Phys. Rev. Lett.* **114**, 110602 (2015).
- [12] R. L. Jack, I. R. Thompson, and P. Sollich, *Phys. Rev. Lett.* **114**, 060601 (2015).
- [13] J. H. Weijs, R. Jeanneret, R. Dreyfus, and D. Bartolo, *Phys. Rev. Lett.* **115**, 108301 (2015).
- [14] E. Tjhung and L. Berthier, *Phys. Rev. Lett.* **114**, 148301 (2015).
- [15] M. Salvalaglio, M. Bouabdellaoui, M. Bollani, A. Benali, L. Favre, J.-B. Claude, J. Wenger, P. de Anna, F. Intonti, A. Voigt, and M. Abbarchi, *Phys. Rev. Lett.* **125**, 126101 (2020).
- [16] D. Hexner and D. Levine, *Phys. Rev. Lett.* **118**, 020601 (2017).
- [17] D. Hexner, P. M. Chaikin, and D. Levine, *Proceedings of the National Academy of Sciences* **114**, 4294 (2017).
- [18] J. H. Weijs and D. Bartolo, *Phys. Rev. Lett.* **119**, 048002 (2017).
- [19] Q.-L. Lei, M. P. Ciamarra, and R. Ni, *Science advances* **5**, eaau7423 (2019).
- [20] Q. Lei and R. Ni, arXiv preprint arXiv:1904.07514 (2019).
- [21] C. E. Zachary and S. Torquato, *Phys. Rev. E* **83**, 051133 (2011).

- [22] S. Torquato, G. Zhang, and F. H. Stillinger, *Phys. Rev. X* **5**, 021020 (2015).
- [23] O. U. Uche, F. H. Stillinger, and S. Torquato, *Phys. Rev. E* **70**, 046122 (2004).
- [24] R. D. Batten, F. H. Stillinger, and S. Torquato, *Journal of Applied Physics* **104**, 033504 (2008).
- [25] R. D. Batten, F. H. Stillinger, and S. Torquato, *Phys. Rev. Lett.* **103**, 050602 (2009).
- [26] J. L. Lebowitz, *Phys. Rev. A* **27**, 1491 (1983).
- [27] G. Zhang, F. H. Stillinger, and S. Torquato, *Phys. Rev. E* **92**, 022119 (2015).
- [28] G. Zhang, F. H. Stillinger, and S. Torquato, *Phys. Rev. E* **92**, 022120 (2015).
- [29] S. Torquato, A. Scardicchio, and C. E. Zachary, *Journal of Statistical Mechanics: Theory and Experiment* **2008**, P11019 (2008).
- [30] R. P. Feynman and M. Cohen, *Phys. Rev.* **102**, 1189 (1956).
- [31] J. A. Sánchez, R. C. Maldonado, M. L. Amigó, G. Nieva, A. Kolton, and Y. Fasano, *Phys. Rev. B* **107**, 094508 (2023).
- [32] M. Hejna, P. J. Steinhardt, and S. Torquato, *Phys. Rev. B* **87**, 245204 (2013).
- [33] R. Xie, G. G. Long, S. J. Weigand, S. C. Moss, T. Carvalho, S. Roorda, M. Hejna, S. Torquato, and P. J. Steinhardt, *Proceedings of the National Academy of Sciences* **110**, 13250 (2013).
- [34] M. A. Klatt, J. Lovrić, D. Chen, S. C. Kapfer, F. M. Schaller, P. W. Schönhofer, B. S. Gardiner, A.-S. Smith, G. E. Schröder-Turk, and S. Torquato, *Nature communications* **10**, 811 (2019).
- [35] Y. A. Gerasimenko, I. Vaskivskiy, M. Litskevich, J. Ravnik, J. Vodeb, M. Diego, V. Kabanov, and D. Mihailovic, *Nat. Mater.* **18**, 1078 (2019).
- [36] S. Sakai, R. Arita, and T. Ohtsuki, arXiv preprint arXiv:2207.09698 (2022).
- [37] Y. Zheng, L. Liu, H. Nan, Z.-X. Shen, G. Zhang, D. Chen, L. He, W. Xu, M. Chen, Y. Jiao, and H. Zhuang, *Sci. Adv.* **6**, eaba0826 (2020).
- [38] D. Chen, Y. Zheng, L. Liu, G. Zhang, M. Chen, Y. Jiao, and H. Zhuang, *Proc. Natl. Acad. Sci. U.S.A.* **118**, e2016862118 (2021).
- [39] D. Chen, Y. Zheng, C.-H. Lee, S. Kang, W. Zhu, H. Zhuang, P. Y. Huang, and Y. Jiao, *Phys. Rev. B* **103**, 224102 (2021).
- [40] Y. Zheng, D. Chen, L. Liu, Y. Liu, M. Chen, H. Zhuang, and Y. Jiao, *Phys. Rev. B* **103**, 245413 (2021).

- [41] D. Chen, Y. Liu, Y. Zheng, H. Zhuang, M. Chen, and Y. Jiao, *Phys. Rev. B* **106**, 235427 (2022).
- [42] H. Zhang, X. Wang, J. Zhang, H.-B. Yu, and J. F. Douglas, arXiv preprint arXiv:2302.01429 (2023).
- [43] D. Chen, X. Jiang, D. Wang, H. Zhuang, and Y. Jiao, *Acta Materialia* **246**, 118678 (2023).
- [44] D. Chen, R. Samajdar, Y. Jiao, and S. Torquato, *Proceedings of the National Academy of Sciences* **122**, e2416111122 (2025).
- [45] W. Shi, Y. Jiao, and S. Torquato, *Phys. Rev. E* **111**, 035310 (2025).
- [46] J. Wang, Z. Sun, H. Chen, G. Wang, D. Chen, G. Chen, J. Shuai, M. Yang, Y. Jiao, and L. Liu, *Phys. Rev. Lett.* **134**, 248301 (2025).
- [47] L. Zhong, S. Mao, and Y. Jiao, *Acta Materialia* , 121218 (2025).
- [48] Y. Jiao, T. Lau, H. Hatzikirou, M. Meyer-Hermann, J. C. Corbo, and S. Torquato, *Phys. Rev. E* **89**, 022721 (2014).
- [49] A. Mayer, V. Balasubramanian, T. Mora, and A. M. Walczak, *Proceedings of the National Academy of Sciences* **112**, 5950 (2015).
- [50] Z. Ge, *Proceedings of the National Academy of Sciences* **120**, e2306514120 (2023).
- [51] Y. Liu, D. Chen, J. Tian, W. Xu, and Y. Jiao, *Phys. Rev. Lett.* **133**, 028401 (2024).
- [52] Y. Tang, X. Li, and D. Bi, arXiv:2408.08976 (2024).
- [53] M. Florescu, S. Torquato, and P. J. Steinhardt, *Proceedings of the National Academy of Sciences* **106**, 20658 (2009).
- [54] W. Man, M. Florescu, K. Matsuyama, P. Yadak, G. Nahal, S. Hashemizad, E. Williamson, P. Steinhardt, S. Torquato, and P. Chaikin, *Optics express* **21**, 19972 (2013).
- [55] W. Man, M. Florescu, E. P. Williamson, Y. He, S. R. Hashemizad, B. Y. Leung, D. R. Liner, S. Torquato, P. M. Chaikin, and P. J. Steinhardt, *Proceedings of the National Academy of Sciences* **110**, 15886 (2013).
- [56] S. Yu, *Nat. Comput. Sci.* **1**, 1 (2023).
- [57] N. Granchi, R. Spalding, M. Lodde, M. Petruzzella, F. W. Otten, A. Fiore, F. Intonti, R. Sapienza, M. Florescu, and M. Gurioli, *Advanced optical materials* **10**, 2102565 (2022).
- [58] S. Park, I. Lee, J. Kim, N. Park, and S. Yu, *Nanophotonics* **11**, 2763 (2021).
- [59] M. A. Klatt, P. J. Steinhardt, and S. Torquato, *Proceedings of the National Academy of Sciences* **119**, e2213633119 (2022).

- [60] N. Tavakoli, R. Spalding, A. Lambertz, P. Koppejan, G. Gkantzounis, C. Wan, R. Rohrich, E. Kontoleta, A. F. Koenderink, R. Sapienza, *et al.*, ACS photonics **9**, 1206 (2022).
- [61] É. Chéron, S. Félix, J.-P. Groby, V. Pagneux, and V. Romero-García, Applied Physics Letters **121**, 061702 (2022).
- [62] S. Yu, C.-W. Qiu, Y. Chong, S. Torquato, and N. Park, Nature Reviews Materials **6**, 226 (2021).
- [63] X. Li, A. Das, and D. Bi, Proceedings of the National Academy of Sciences **115**, 6650 (2018).
- [64] G. Zhang, F. Stillinger, and S. Torquato, The Journal of chemical physics **145**, 244109 (2016).
- [65] S. Torquato, Phys. Rev. E **104**, 054102 (2021).
- [66] C. E. Maher, F. H. Stillinger, and S. Torquato, Phys. Rev. Mater. **6**, 025603 (2022).
- [67] Y. Xu, S. Chen, P.-E. Chen, W. Xu, and Y. Jiao, Phys. Rev. E **96**, 043301 (2017).
- [68] J. Puig, F. Elías, J. Aragón Sánchez, R. Cortés Maldonado, G. Rumi, G. Nieva, P. Pedrazzini, A. B. Koltun, and Y. Fasano, Communications Materials **3**, 32 (2022).
- [69] S. Torquato and D. Chen, Multifunctional Materials **1**, 015001 (2018).
- [70] J. Kim and S. Torquato, Proceedings of the National Academy of Sciences **117**, 8764 (2020).
- [71] S. Torquato, Journal of Composite Materials **56**, 3635 (2022).
- [72] J. A. Loera, J. Rambau, and F. Santos, *Triangulations: Structures for Algorithms and Applications*, 2nd ed. (Springer Berlin, Heidelberg, 2010).
- [73] H. Yuan, H. Chen, M. Li, J. Lin, and L. Liu, Phys. Rev. Lett. **136**, 087101 (2026).
- [74] S. Torquato and Y. Jiao, Phys. Rev. E **87**, 022111 (2013).
- [75] D. S. Callaway, M. E. J. Newman, S. H. Strogatz, and D. J. Watts, Phys. Rev. Lett. **85**, 5468 (2000).
- [76] R. Cohen, K. Erez, D. ben Avraham, and S. Havlin, Phys. Rev. Lett. **85**, 4626 (2000).
- [77] S. N. Dorogovtsev, A. V. Goltsev, and J. F. F. Mendes, Rev. Mod. Phys. **80**, 1275 (2008).
- [78] P. Mann, V. A. Smith, J. B. O. Mitchell, and S. Dobson, Phys. Rev. E **106**, 014304 (2022).
- [79] E. Newby, W. Shi, Y. Jiao, R. Albert, and S. Torquato, Phys. Rev. E **111**, 034123 (2025).
- [80] E. Newby, W. Shi, Y. Jiao, S. Torquato, and R. Albert, Journal of Complex Networks **13** (2025).
- [81] A. Weinrib and B. I. Halperin, Phys. Rev. B **27**, 413 (1983).
- [82] A. Weinrib, Phys. Rev. B **29**, 387 (1984).
- [83] A. B. Harris, Journal of Physics C: Solid State Physics **7** (1974).

- [84] S. Prakash, S. Havlin, M. Schwartz, and H. E. Stanley, Phys. Rev. A **46**, R1724 (1992).
- [85] K. J. Schrenk, N. Posé, J. J. Kranz, L. V. M. van Kessenich, N. A. M. Araújo, and H. J. Herrmann, Phys. Rev. E **88**, 052102 (2013).
- [86] S. Torquato, Appl. Mech. Rev. **55**, B62 (2002).
- [87] E. C. Oğuz, J. E. S. Socolar, P. J. Steinhardt, and S. Torquato, Phys. Rev. B **95**, 054119 (2017).
- [88] C. E. Zachary and S. Torquato, J. Stat. Mech. Theor. Exp. **2009**, P12015 (2009).
- [89] D. Chen and S. Torquato, Acta Mater. **142**, 152 (2018).
- [90] G. Zhang, F. H. Stillinger, and S. Torquato, Phys. Rev. E **96**, 042146 (2017).
- [91] C. E. Zachary, Y. Jiao, and S. Torquato, Phys. Rev. E **83**, 051308 (2011).
- [92] C. E. Zachary, Y. Jiao, and S. Torquato, Phys. Rev. E **83**, 051309 (2011).
- [93] J. Kim and S. Torquato, Phys. Rev. B **97**, 054105 (2018).
- [94] G. Zhang, F. H. Stillinger, and S. Torquato, Soft Matter **13**, 6197 (2017).
- [95] F. Iannelli, A. Koher, D. Brockmann, P. Hövel, and I. M. Sokolov, Phys. Rev. E **95**, 012313 (2017).
- [96] D. Brockmann and D. Helbing, Science **342**, 1337 (2013).
- [97] J. Senk, B. Kriener, M. Djurfeldt, N. Voges, H.-J. Jiang, L. Schüttler, G. Gramelsberger, M. Diesmann, H. E. Plesser, and S. J. van Albada, PLOS Computational Biology **18**, 1 (2022).
- [98] A. Perinelli, D. Tabarelli, C. Miniussi, and L. Ricci, Scientific Reports **9**, 13412 (2019).
- [99] D. Stauffer and A. Aharony, *Introduction to percolation theory* (Taylor and Francis, London, 1994).
- [100] F. Yonezawa, S. Sakamoto, and M. Hori, Phys. Rev. B **40**, 636 (1989).
- [101] M. E. J. Newman and R. M. Ziff, Phys. Rev. E **64**, 016706 (2001).
- [102] S. Mertens and C. Moore, Phys. Rev. E **86**, 061109 (2012).
- [103] S. Mitra, I. Mukherjee, and P. K. Mohanty, Phys. Rev. E **112**, 014120 (2025).
- [104] C. E. Maher and K. A. Newhall, Phys. Rev. E **111**, 065420 (2025).
- [105] M. E. J. Newman, S. H. Strogatz, and D. J. Watts, Phys. Rev. E **64**, 026118 (2001).
- [106] S. Torquato, O. U. Uche, and F. H. Stillinger, Phys. Rev. E **74**, 061308 (2006).
- [107] G. Zhang and S. Torquato, Phys. Rev. E **88**, 053312 (2013).